Multi-angular Multispectral Sensing of Barley Awn Coloring

MORITZ CAMENZIND[1], MICHAEL THALER[1], ULF FEUERSTEIN[2] & KANG YU[1]

Abstract: Barley awn coloring is a descriptive trait for barley (Hordeum vulgare) testing by the European Union. Rating the coloring visually is difficult and measuring canopy reflectance by a multispectral canopy might be more accurate. Reflectance of barley canopies with different awn coloring levels was measured from different viewing angles using a multispectral camera mounted to an unmanned aerial vehicle. The bi-directional reflectance distribution of the canopies was determined and used for deriving the anthocyanin reflection index, which was then used to identify the optimal viewing angles for the detection of Barley awn coloring. The index differed between the canopies without awn coloring and the canopies with awn coloring. The proposed method failed to detect subtle changes of awn coloring but it might be further improved and used to characterize canopy traits from multiple viewing angles.

1 Introduction

Barley awn coloring is a result of the accumulation of color pigments such as anthocyanins in the barley awn tips during flowering. It is a descriptive trait for barley (*Hordeum vulgare*) plants during the testing process for distinctness, uniformity and stability by the community plant variety office (CPVO) of the European Union. The coloring is usually rated visually, which is difficult because barley awn coloring is very subtle, is only present during a short time period and its perception depends on the viewing geometry of the examiner. Barley awn coloring might be measured with a higher consistency and accuracy by multispectral reflectance measurements of the canopy. Experience from visually rating barley awn coloring suggests that a viewing zenith angle that is higher than nadir might be beneficial for the detection of barley awn coloring with multispectral cameras as well.

Multispectral reflectance of canopies is widely used in agriculture remote sensing to estimate e.g. nitrogen use efficiency (ARGENTO et al. 2021) or green fraction (JAY et al. 2017). Often, canopy reflectance is measured from nadir by using a Structure from Motion (SfM) algorithm, which stiches pixels of single images into an orthomosaic. However, canopy reflectance is highly dependent on the geometry of observation (SANDMEIER & ITTEN 1999) and can be described by a bi-directional reflectance distribution function (NICODEMUS et al. 1977). Models accounting for the effects of bi-directional reflectance distribution (BRD) have been used to observe the leaf area index (LAI) and chlorophyll content (ROOSJEN et al. 2018) as well as reproductive organs (LI et al. 2021).

The data collection as well as the data processing have to be adjusted from measurement procedures used for the collection of nadir observations when measuring BRD using a multispectral camera mounted to an unmanned aerial system (UAS). LI et al. (2021) adjusted the flight path, which limited the area that can be covered by a single flight to few hundred square meters. ROOSJEN et al. (2018) down sampled the image resolution to a ground sampling distance of 5 m to calculate viewing angles for single pixels. Both approaches are limited at measuring BRD

[1] Technical University of Munich, Chair of Precision Agriculture, Dürnast 9, D-85354 Freising
E-Mail: [moritz.camenzind, michael.david.thaler, kang.yu]@tum.de
[2] Deutsche Saatveredelung AG, Steimker Weg 7, D-27330 Asendorf
E-Mail: ulf.feuerstein@dsv-saaten.de

 DOI: 10.24407/KXP:1795645911

for trials with several hundred plots of a size of few square meters as can be found in breeding trials.
A workflow to extract LAI from multi-view RGB images developed by ROTH et al. (2018) was adjusted to cope with multispectral images in order to measure canopy BRD of barley canopies during the appearance of awn coloring. The BRD was then used to identify the optimal viewing configuration to detect barley awn coloring by canopy reflectance measurements.

2 Materials and Methods

All measurements were taken at the breeding station of the Deutsche Saatveredelung AG (DSV) in Asendorf, Lower Saxony, Germany (52.777° N, 8.682° E, 50 m a.s.l.). A total number of 150 Barley (*Hordeum vulgare*) genotypes were drill sown in plots of 1.5 m × 5 m size, which were placed randomly in a grid on the trial site. Fertilization and plant protection were carried out according to local practice. The anthocyanin coloring of the awns was rated visually according to a protocol used by the European Union for variety testing (COMMUNITY PLANT VARIETY OFFICE 2019; Tab. 1). The BBCH stage of the canopies was 60 to 65 during measurements and the expression of the barley awn coloring was maximal.

Tab. 1: Definitions of the rating scores.

Score	Definition
1	no awn coloring
3	single awns were colored but no homogenous coloring
5	light awn coloring
7	intermediate awn coloring
9	strong awn coloring

The multispectral images were taken using a MicaSense Altum camera (MicaSense Inc., Seattle, USA), which has five bands (475 nm, 560 nm, 668 nm, 717 nm and 842 nm) and a field of view of 48° × 37°. The camera was mounted on a Matrice 600 Pro rotary wing unmanned aerial system (Dà-Jiāng Innovations Science and Technology Company, Shenzhen, China). During flight, the camera was oriented in nadir and the width of the sensor was aligned to flight direction, which was east-east-south to west-west-north and the opposite direction. Flight height was 37 m above ground level, resulting in a ground sampling distance (GSD) of 16 mm. Flight speed was 1.6 m s^{-1}, front and side overlap were 90%. The flight took place under stable and sunny weather conditions on May 31, 2021 at 12:48 local time (UTC + 1) and lasted 11 min.
Goal of the image processing was to obtain reflectance values from single plots defined by ROIs on single images (Fig. 1). As a first step, the images were calibrated geometrically as well as radiometrically. The geometric calibration included distortion correction, the radiometric calibration included corrections for vignette, black level, exposure and gain. Radiance was converted into reflectance by measuring the radiance of a panel with a known reflectance before and after the flight. Calibration values during the flight were linearly interpolated. Finally, the images of single bands were co-registered. The mentioned steps were all carried out using python code (Python Software Foundation, https://www.python.org/), which was provided by the camera manufacturer (MICASENSE, 2021).

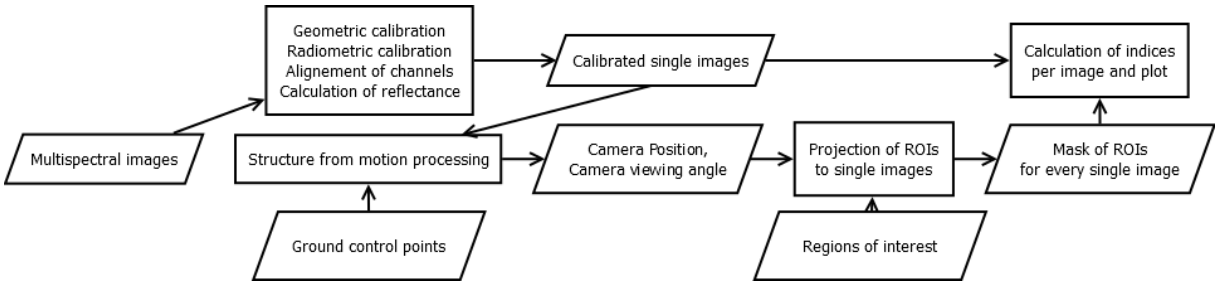

Fig 1: Diagram of the applied Workflow

After calibration, the images were imported into Agisoft Metashape Professional 1.7.2 (Agisoft LLC, St. Petersburg, Russia) and processed as described by ROTH et al. (2018). The coordination system used was ESPG: 32632 (WGS 84 / UTM zone 32N), size of the ROIs, containing information about the location of the plots, was 1.1 m × 4.4 m. After processing, a geojson file was exported containing information about the position of the plots in each single image, as well as on the viewing geometry, such as the viewing azimuth and the viewing zenith angle.
In order to detect barley awn coloring the anthocyanin reflection index (ARI) was calculated on a pixel basis according to GITELSON et al. (2001):

$$ARI = \frac{1}{R_{560}} - \frac{1}{R_{717}}$$

where R is the reflectance of the respective wavelength. A median was calculated per plot, image, band or index, including all the pixels within the ROI.
Further data analysis and plotting was done in R 4.0.5 (R CORE TEAM, 2021). To produce a visual representation of the BRD, the reflection measurements of single plots were interpolated using inverse distance weighing. Only measurements that were taken from azimuth angles relative to the sun of – 10° to 10° and 170° to 190° and zenith angles of more than 11° were considered for comparison of the rating with the reflectance measurement. Within these regions, the ARI was not dependent on the viewing angles. Analysis of variance and the Tukey post hoc test were carried out on a significance level of 5 %.

3 Results

The visual rating of the barley awn coloring found 77 plots, which showed no awn coloring, 15 plots where single awns were colored, 21 plots with light awn coloring, 31 plots with intermediate awn coloring and 5 plots with high awn coloring. Imaging yielded 304 image stacks, on each stack we located 30 plots on average (sd = 15). We therefore obtained 9084 single measurements per band or index, resulting in an average of 60 measurements per plot (sd = 9). Plots located in the middle of the trial were measured more often than those at the border. Viewing azimuth angles ranged from 0° to 360°, most measurements were made perpendicular to flight direction. Viewing zenith angles range from 0° to 28°, most measurements were taken at a viewing zenith angle of 12°.
A lower reflectance in the green band was measured for plots with a rated awn coloring of 1 (0.032, cv = 27.6) compared to plots with a rated awn coloring of 9 (0.029, cv = 26.1). Reflectance in the rededge band was similar for both awn color ratings (0.089, cv = 18.7 and 0.090, cv = 17.0). The ARI was lower for plots with an awn color rating of 1 (21.4, cv = 29.9) compared to a rating of 9 (24.8, cv = 28.8).

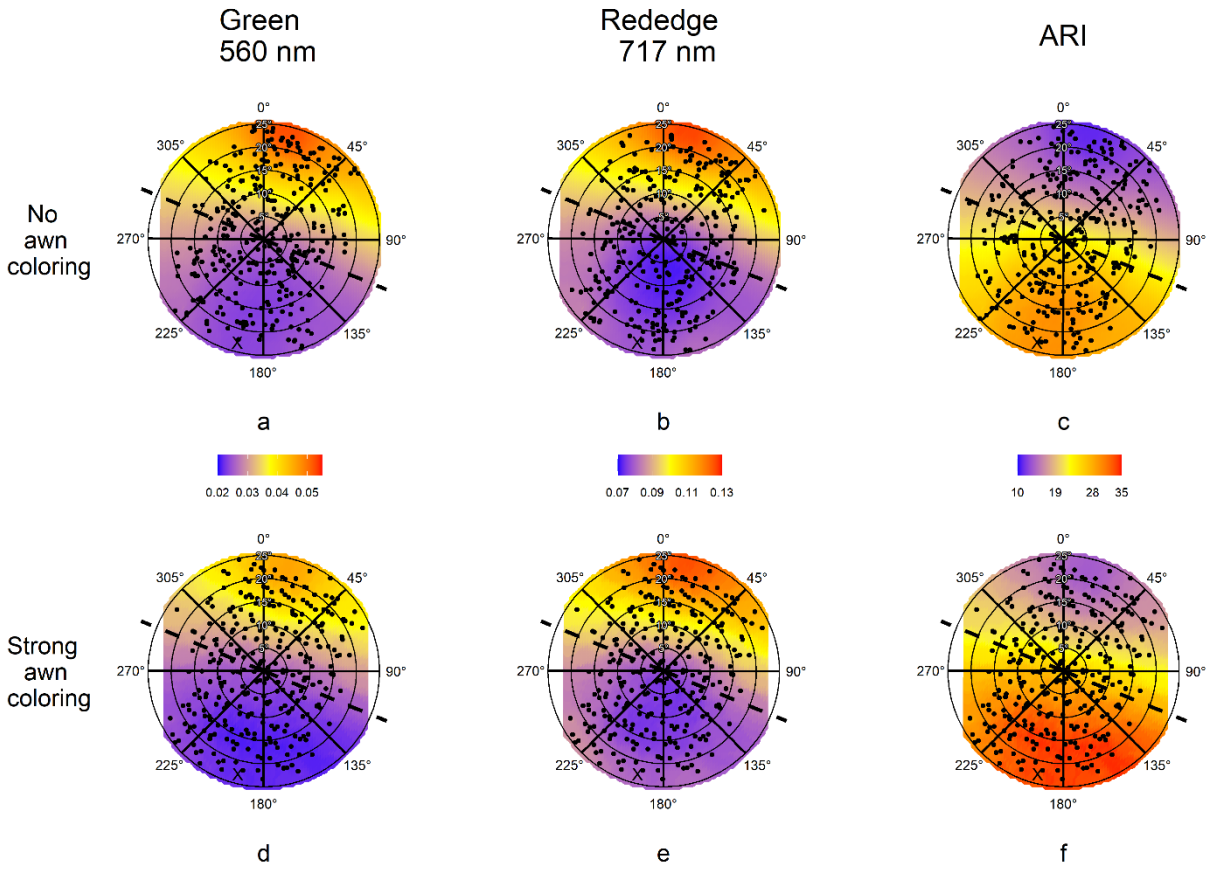

Fig. 2: Representation of the measured BRD from all plots with no (Rating 1, top) and high awn coloring (Rating 9, bottom). (a, c) represent the green, (b, c) the rededge and (c, f) the ARI BRD. The x-axis displays the viewing azimuth angle (0 ° corresponds to north, 90 ° to east), the y-axis corresponds to the viewing zenith angle. The black cross represents the sun azimuth position, the black dashed line the direction of flight. The black dot represent locations of measurements of which only 300 measurements are shown per subfigure to make the figure more readable. Images were taken at 12:48 local time (UTC + 1).

The reflectance in both bands decreased with the viewing azimuth angle relative to the sun (Fig. 2). The reflection in the rededge band was further negatively correlated with the zenith viewing angle (Fig. 2b). The same effect was observed in the near-infrared band, where the effect was more distinct (data not shown). The ARI increased with a lower viewing azimuth angle relative to the sun (Fig. 2cd) and was maximal when the angle is 0 ° and minimal for a viewing azimuth angle relative to the sun of 180 °. A positive relationship between the viewing zenith angle and the ARI was found when filtering for viewing azimuth angles relative to the sun of 350 ° to 10 ° and 170 ° to 190 °. The variability in the ARI however increased with the viewing zenith angle (Fig. 3c).

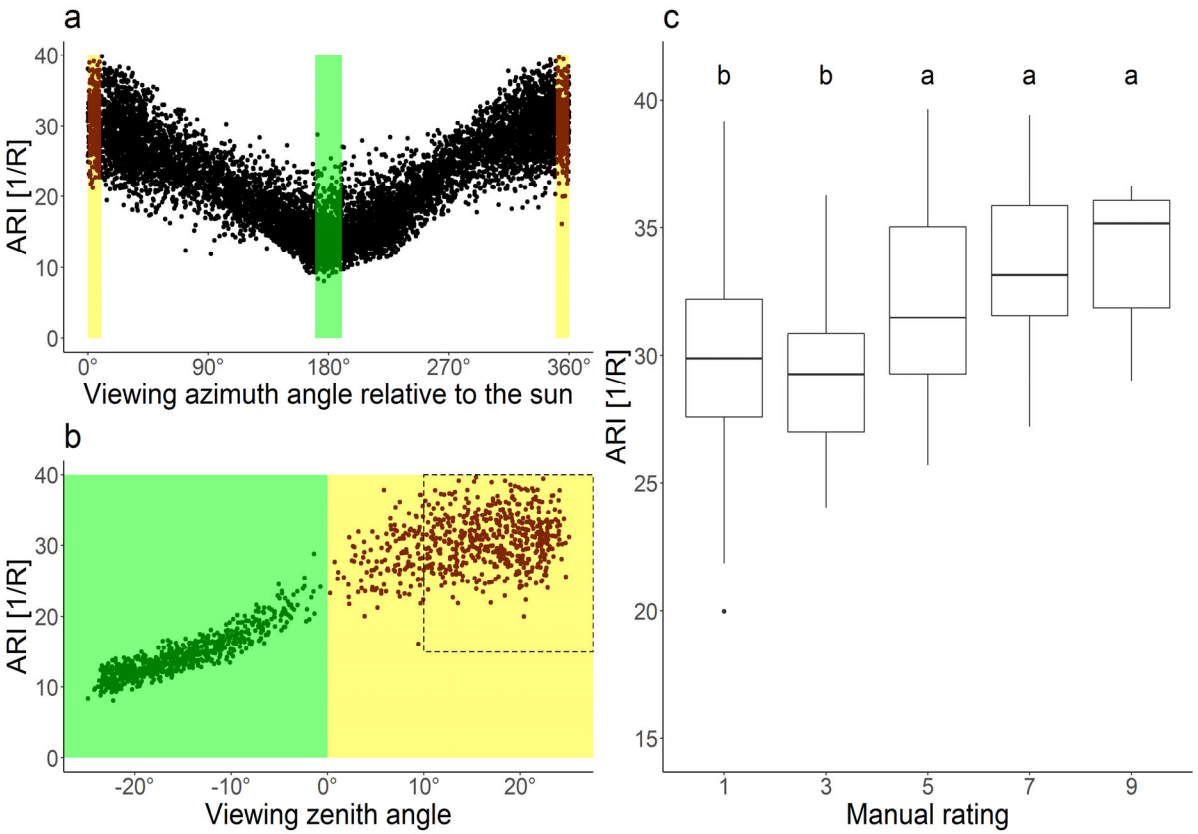

Fig. 3: Influence of viewing angles on the ARI (a, b) as well as the ARI of different rating groups (c). (a) shows the influence of the viewing azimuth angle relative to the sun, where 0 ° is the forward and 180 ° is the backward scattering direction. The colored areas display the region from which the values were filtered for further analysis. (b) shows the influence of the viewing zenith angle at the mentioned viewing azimuth angles. Negative angles correspond to zenith angles in the backward scattering direction, positive angles to the forward scattering direction. Colored regions correspond to (a), the dashed line box includes values with a viewing zenith angle of 11 ° and more. (c) displays the ARI for measurements filtered by the mentioned viewing azimuth and viewing zenith angles grouped by their rating score. The letters correspond to the statistical group of the Tukey comparisons.

After filtering for the aforementioned sun azimuth angles and viewing zenith angles of more than 11 °, significant differences were found in the ARI between plots where no or only single awns were colored and plots where the awns were colored (Fig. 3c). For viewing zenith angles of more than 0 ° and less than 11 ° no significant differences among the rating groups in the ARI were found (Data not shown).

4 Discussion and Outlook

Adapting the workflow developed by ROTH et al. (2018) to multispectral imaging was successful. The importance of choosing the same viewing geometry when comparing reflectance measurements is underlined by the relatively big coefficient of variation (cv) for measurements of a single rating group including all viewing angles. Differences in the mean of the ARI between rating groups are much smaller than within the group.

Tab. 2: Statistical parameters of ARI measurements per rating group

Rating	1	3	5	7	9
n	220	62	65	119	12
ARI mean	29.7	29.0	32.2	33.4	33.9
ARI cv	11.2	9.3	311.6	8.4	7.7

Generally, the reflectance decreased with a lower viewing angle relative to the sun and increased with increasing viewing angle (Fig. 2). The highest reflectance was measured with a viewing angle relative to the sun of around 180°. The measured BRD therefore stands in opposition to other studies, which found an increasing reflectance in the single bands with a lower azimuth angle relative to the sun (BURKART et al. 2015; LI et al. 2021). One reason for the unexpected BRD might be due to the image reflectance calibration. We initially planned to calibrate the images using an incident light sensor (ILS) mounted to the UAS. However, the irradiation measured by the ILS was highly affected by the yaw angle of the UAV and therefore not suitable for reflectance calibration on single images. Using reflectance panels on the ground is a well-known approach for the radiometric calibration of multispectral images but was limited to one calibration image before and one calibration image after the flight. A calibration with the method used, requires perfectly stable light conditions, which are rare in Lower Saxony. For future flight campaigns, reflectance panels should be put within the trial site to calibrate each image individually. These panels will further allow to calculate a bi-directional reflectance distribution function (BRDF) of the canopies.
Further, the BRD of canopies with colored barley awns might be different than the BRD of canopies measured in other studies. LI et al. (2021) measured the BRD of wheat at a similar BBCH stage, when awns were present in the canopy as well but the awns were not colored. We might therefore review our findings in a next study, measuring the BRD using established techniques for BRD measurements such as a hand held hyperspectrometer.
The optimal viewing angle range should be as narrow as possible to exclude viewing angle effects within the selected range. However, the range needs to be big enough in order to obtain enough reflectance measurements. We found that the ARI measurements stay stable in relation to the viewing azimuth angle in ranges with a size 20° centered on a sun azimuth angle of 0° and on a sun azimuth angle of 180° (Fig. 3). The ARI in these viewing azimuth angle ranges is highly correlated to the viewing zenith angle. Therefore, as for the viewing zenith angle, a range has to be chosen to obtain comparable measurements. We filtered the dataset for a viewing zenith angle of more than 11°, since the values in this range do not change significantly with the viewing zenith angle. Using this viewing configuration yielded significant differences in the ARI between the plots with non-colored and the plots with colored awns. Still, the variability in the ARI within one level of rated awn coloring is very high and an ARI measurement cannot clearly be assigned to a rating group, making it difficult to use the procedure in practice (Tab. 2). The detection might be improved by a higher viewing zenith angle. Currently, the viewing zenith angles are limited by the field of view of the camera and have not been high enough to measure the full BRD and observing phenomena such as the hot spot effect (KUUSK 1991). This shortcoming might be solved by tilting the camera on the UAV or choosing a flight time when the sun zenith angle is higher. Another improvement to the workflow would be the use of smaller ROIs. The used ROIs have almost the same size as the plot and the viewing angles of single pixels within one ROI vary by several degrees. Using smaller ROIs would

allow for smaller variation in the viewing angles within the ROI and therefore allow choosing the viewing angles more precisely. Smaller ROIs would however be less representative for the whole plot.
Using the proposed method for multi-angular multispectral measurements for canopy reflectance measurements shows promising first results. The method might be further improved and used to characterize canopy traits from multiple viewing angles. However, compared to classical reflectance measurements, the proposed method is more complex and requires optimal measuring conditions as well as further improvements.

5 Acknowledgements

We thank the Deutsche Saatveredelung AG (DSV) for providing access to their breeding trial as well as to their infrastructure for data collection.

6 Literature

ARGENTO, F., ANKEN, T., ABT, F., VOGELSANGER, E., WALTER, A. & LIEBISCH, F., 2021: Site-specific nitrogen management in winter wheat supported by low-altitude remote sensing and soil data. Precision Agriculture, **22**(2), 364-386, https://doi.org/10.1007/s11119-020-09733-3.

BURKART, A., AASEN, H., ALONSO, L., MENZ, G., BARETH, G. & RASCHER, U., 2015: Angular Dependency of Hyperspectral Measurements over Wheat Characterized by a Novel UAV Based Goniometer. Remote Sensing, 7(1), 725-746, https://doi.org/10.3390/rs70100725.

COMMUNITY PLANT VARIETY OFFICE, 2019: Protocol for distinctness, uniformity and stability tests. Angers, France, https://cpvo.europa.eu/sites/default/files/documents/hordeum_5_0.pdf.

GITELSON, A. A., MERZLYAK, M. N. & CHIVKUNOVA, O. B., 2001: Optical properties and nondestructive estimation of anthocyanin content in plant leaves. Photochem Photobiol, **74**(1), 38-45, https://www.doi.org/10.1562/0031-8655(2001)074%3C0038:OPANEO%3E2.0.CO;2.

JAY, S., MAUPAS, F., BENDOULA, R. & GORRETTA, N., 2017: Retrieving LAI, chlorophyll and nitrogen contents in sugar beet crops from multi-angular optical remote sensing: Comparison of vegetation indices and PROSAIL inversion for field phenotyping. Field Crops Research, **210**, 33-46, https://doi.org/10.1016/j.fcr.2017.05.005.

KUUSK, A., 1991: The Hot Spot Effect in Plant Canopy Reflectance. In R. B. Myneni & J. Ross (Eds.), Photon-Vegetation Interactions: Applications in Optical Remote Sensing and Plant Ecology, 139-159, Springer Berlin Heidelberg, https://doi.org/10.1007/978-3-642-75389-3_5.

LI, W., JIANG, J., WEISS, M., MADEC, S., TISON, F., PHILIPPE, B., COMAR, A. & BARET, F., 2021: Impact of the reproductive organs on crop BRDF as observed from a UAV. Remote Sensing of Environment, **259**, 112433, https://doi.org/10.1016/j.rse.2021.112433.

MICASENSE, 2021: MicaSense RedEdge and Altum Image Processing Tutorials. Micasense Inc., https://github.com/micasense/imageprocessing.

NICODEMUS, F.E., KICLUNOND, J.C., HSIA, J.J., GINSBERG, I.W., LIMPERIS, T., 1977: Geometrical Considerations and Nomenclature for Reflectance (no. NBS MONO 160). National Bureau of Standards, Gaithersburg, MD, https://doi.org/10.6028/NBS.MON0.160.

R CORE TEAM, 2021: R: A Language and Environment for Statistical Computing. R foundation for statistical computing, Vienna, Austria, https://www.R-project.org/.

ROOSJEN, P. P. J., BREDE, B., SUOMALAINEN, J. M., BARTHOLOMEUS, H. M., KOOISTRA, L. & CLEVERS, J. G. P. W., 2018: Improved estimation of leaf area index and leaf chlorophyll content of a potato crop using multi-angle spectral data – potential of unmanned aerial vehicle imagery. International Journal of Applied Earth Observation and Geoinformation, **66**, 14-26, https://doi.org/10.1016/j.jag.2017.10.012.

ROTH, L., AASEN, H., WALTER, A. & LIEBISCH, F., 2018: Extracting leaf area index using viewing geometry effects—A new perspective on high-resolution unmanned aerial system photography. ISPRS Journal of Photogrammetry and Remote Sensing, **141**, 161-175, https://doi.org/10.1016/j.isprsjprs.2018.04.012.

SANDMEIER, S. R. & ITTEN, K. I., 1999: A field goniometer system (FIGOS) for acquisition of hyperspectral BRDF data. IEEE Transactions on Geoscience and Remote Sensing, **37**(2), 978-986, https://doi.org/10.1109/36.752216.